



Structures and relative stabilities of Na^+Ne_n ($n = 1-16$) clusters via pairwise and DFT calculations

Mouna Ben Hadj Ayed¹ · Tringa Osmani² · Nouredine Issaoui¹ · Avni Berisha² · Brahim Oujja³ · Houcine Ghalla¹

Received: 16 January 2019 / Accepted: 31 May 2019 / Published online: 5 June 2019
© Springer-Verlag GmbH Germany, part of Springer Nature 2019

Abstract

The structural properties and relative stabilities of the Na^+Ne_n clusters, with $n = 1-16$, have been investigated by using pairwise and density functional theory (DFT) methods. The DFT calculations have been carried out using the M06-2X functional combined with the augmented aug-cc-pVTZ basis sets. For both methods, the high stability is obtained for $\text{Na}^+\text{Ne}_{12}$ cluster with an icosahedral structure, and the twelve Ne atoms complete the first solvation shell around the Na^+ cation. Therefore, the icosahedral $\text{Na}^+\text{Ne}_{12}$ structure will be considered as the core for the larger sizes. The relative stabilities have been studied in terms of the binding energies, second-order difference of energies, fragmentation energies and HOMO–LUMO energy gaps. The Na–Ne interactions within the Na^+Ne_n clusters in relation to the relative stabilities have been discussed through topological atom-in-molecules and reduced density gradient analyses. Finally, the relative stabilities of the Na^+Ne_n clusters have been discussed topologically.

Keywords Na^+Ne_n · Relative stabilities · Pairwise · DFT calculations · M06-2X · Non-covalent interactions

1 Introduction

Van der Waals interactions between rare gas and alkali ions have been frequently studied thanks to the closed shell structure of the noble gas atoms. The study of interactions within clusters and their stabilities is of great importance to understand many phenomena such as nucleation, phase transition and solvation. Also, these mixed clusters are helpful to understand the evolution of many optical, chemical and physical properties from the microscopic levels to the bulk [1]. Cationic clusters M^+Rg_n (where M is a metal atom and Rg is a rare gas) have been studied both experimentally [1–10] and theoretically [1–4, 11–48]. Experimentally, the mass spectrometry method is the most used to evaluate the stabilities of these complexes. The mass spectra obtained

by Luder et al. [6] for Na^+Ar_n clusters show the following magic number at $n = 6, 8, 10, 13, 16, 20, 23, 25$ which refer to the most stable clusters. These numbers were analyzed by Velagrakis et al. [1, 4, 6]. The growing pattern of these clusters consists of a self-arrangement in shells around the centered cation M^+ to reach the first solvation layer. At this defined size, we obtain the most stable cluster. In this context, five structures have been found: We quote the tetrahedron for $n = 4$, the octahedron for $n = 6$, the square antiprism for $n = 8$, the capped square antiprism for $n = 10$ and the icosahedron for $n = 12$ [1, 4, 6]. The change of cluster geometry as a function of size presents an interesting matter. In fact, the crystals of rare gas exhibit a faced centered cubic structure, whereas clusters with size less than 1000 atoms adopt icosahedral structure [9, 10]. Theoretically, various methods have been implemented to investigate the geometries of the different types of clusters. The most successful methods are those of the basin hopping method into the Monte Carlo simulation [11–13, 30, 40–43] and the genetic algorithm [45–48]. The DFT calculations have been also well used to analyze different cluster systems, particularly in the case of metal clusters such as CuSi_n [27, 31, 39], Au_nBe and Au_nBe_2 [33], Ge_nAl [32], Fe_nN [36], AuSi_n [37] and Fe_nCr [38]. In the present work, the stable geometries of the Na^+Ne_n clusters have been investigated by using pairwise method and

✉ Houcine Ghalla
houcineghalla@yahoo.fr

¹ Quantum and Statistical Physics Laboratory, Faculty of Sciences, University of Monastir, Monastir, Tunisia

² Chemistry Department of Natural Sciences Faculty, University of Prishtina, rr. “Nena Tereze” nr. 5, 10000 Prishtina, Kosovo

³ Physics Department, Faculty of Science, University of Jeddah, Jeddah, Kingdom of Saudi Arabia

DFT calculations. The relative stabilities of Na^+Ne_n clusters are discussed based on different energetic quantities, such as bending energy, second-order energy difference, fragmentation energy, HOMO–LUMO gap energy and dipole moment. Topological AIM analysis of Na–Ne interactions have been reported and discussed in connection with the stabilities of the Na^+Ne_n clusters.

2 Computational methods

The geometry optimizations of the Na^+Ne_n clusters have been performed by using the basin hopping global optimization and DFT methods. For the first method, we have used the pairwise potential to describe the potential energy surface of the clusters. The pairwise potential is an additive model where the total energy is obtained by a simple addition of the $\text{Na}^+\text{–Ne}$ and Ne–Ne interaction potentials:

$$V_{\text{Tot}}(r) = \sum_{i=1}^n V_{\text{Na}^+\text{–Ne}}(r_{0i}) + \sum_{i=1}^n \sum_{i<j} V_{\text{Ne–Ne}}(r_{ij}) \quad (1)$$

The $V_{\text{Ne–Ne}}$ potential is obtained from the Lennard-Jones one:

$$V_{\text{Ne–Ne}}(r_{ij}) = 4\varepsilon \left[\left(\frac{\sigma}{r_{ij}} \right)^{12} - \left(\frac{\sigma}{r_{ij}} \right)^6 \right] \quad (2)$$

where ε and σ are the well depth and the equilibrium distance, respectively. These quantities are $\varepsilon = 0.00011399$ a.u. and $\sigma = 5.10$ a.u. The $V_{\text{Na}^+\text{–Ne}}$ potential is taken from the numerical form [49] using the analytical form of Tang and Toennies [50]:

$$V_{\text{Na}^+\text{–Ne}}(r) = A_{\text{eff}} \exp(-br) - \frac{D_4 \alpha_{\text{Ne}}}{r^4} - \frac{D_6}{r^6} - \frac{D_8}{r^8} - \frac{D_{10}}{r^{10}} \quad (3)$$

The exponential term describes the short-range repulsion interactions, while the remaining terms express the long-range dispersion ones. The parameters A_{eff} , b , D_4 , D_6 , D_8 and D_{10} result from the square fitting of the numerical potential [49]. The $\alpha_{\text{Ne}} = 2.663 a_0^3$ is the neon's polarizability.

The DFT calculations have been carried out with the M06-2X exchange–correlation functional and the augmented basis sets aug-cc-pVTZ, as implemented in Gaussian 09 package [51]. Before the optimization, we have used the artificial bee colony (ABC) algorithm which is incorporated into ABCluster algorithm [52, 53] to search the lowest energy structures of Na^+Ne_n clusters. The Lennard-Jones potential has been used for the research of global minimum. For the small cluster sizes $n \leq 6$, 100 initial configurations were generated, and from $n = 7$, more than 500 guess structures are generated. For each size, the geometry having the

lowest energy is then optimized with DFT calculations. The M06-2X functional is a reliable hybrid functional, and it has been developed by Zhao et al. [54, 55]. In fact, this functional is suitable to describe the non-covalent interactions and it is able to provide accurate binding energies. In order to test the reliability of our DFT calculations, some test calculations are carried out on $\text{Na}^+\text{–Ne}$ and Ne–Ne using B3LYP, B3PW91 and M06-2X functionals with 6-311(d), 6-311++(d,p), aug-cc-pVDZ and aug-cc-pVTZ basis sets. The calculated $\text{Na}^+\text{–Ne}$ and Ne–Ne bond lengths and available experimental data are listed in Table 1. Comparing with the experimental data [56, 57], we can conclude that M06-2X functional combined with aug-cc-pVTZ basis set is more optimal than others.

3 Results and discussion

3.1 Lowest energy structures

The lowest energy structures of Na^+Ne_n clusters computed by the pairwise method and DFT calculations are depicted in Figs. 1 and 2, respectively. The $\text{Na}^+\text{–Ne}$ and Ne–Ne bond lengths in each cluster are regrouped in Table 2. For the Na^+Ne dimer, Na^+ and Ne are distant by 2.413 and 2.508 Å for the pairwise and DFT methods, respectively. The trimer Na^+Ne_2 shows an isosceles triangular geometry (C_{2v} symmetry) with vertex Na^+ . The tetramer Na^+Ne_3 cluster has C_{3v} symmetry and exhibits that a pyramidal structure with the Na^+ ion is on the summit.

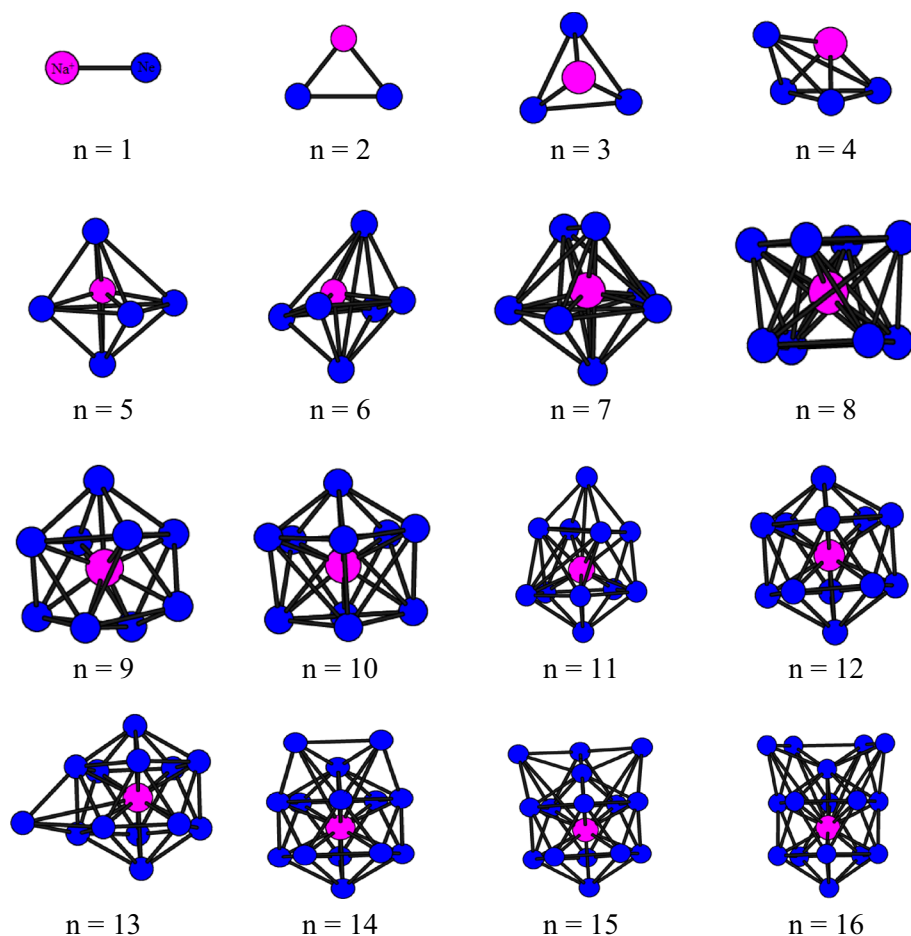
The Na^+Ne_4 cluster shows a bipyramid structure with the C_{3v} symmetry by using the pairwise method and a tetrahedron structure with T_d symmetry with the DFT calculations. The Na^+Ne_6 cluster shows two distinctly different

Table 1 Computed $\text{Na}^+\text{–Ne}$ and Ne–Ne bond lengths (Å) and available experimental data

Methods	$\text{Na}^+\text{–Ne}$	Ne–Ne
Experiment	2.500 ^a	3.100 ^b
M06-2X/aug-cc-pVTZ	2.508	3.017
B3LYP/aug-cc-pVTZ	2.484	3.100
B3PW91/6-311(d)	2.470	3.138
M06-2X/aug-cc-pVDZ	2.530	2.979
B3LYP/6-311++(d,p)	2.533	3.144
M06-2X/6-311++(d,p)	2.537	2.985
B3LYP/aug-cc-pVDZ	2.558	3.541
M06-2X/6-311(d)	2.407	2.693
B3PW91/6-311++(d,p)	2.69	3.947
B3LYP/6-311(d)	2.369	2.651
B3PW91/aug-cc-pVDZ	2.720	4.570

^a[56], ^b[57]

Fig. 1 Lowest energy geometries of Na^+Ne_n ($n = 1-16$) clusters obtained by the pairwise method



geometries. We obtained a pentagonal geometry using DFT calculations and an undefined with a pairwise approach. For the Na^+Ne_8 cluster, both methods have shown a square antiprism structure with D_{4h} symmetry. The $\text{Na}^+\text{Ne}_{10}$ cluster obtained by the pairwise method presents a double-crown structure; the upper and lower ones possess five and four Ne atoms, respectively. However, the DFT calculations converged to a capped square antiprism structure. The $\text{Na}^+\text{Ne}_{11}$ cluster is obtained by adding only one Ne atom to the lower side of $\text{Na}^+\text{Ne}_{10}$ found via the pairwise method.

As clearly seen, in Figs. 1 and 2, the deposition of the neon atoms gradually leads to the formation of the first solvation layer. For both methods, the first solvation layer is obtained for $\text{Na}^+\text{Ne}_{12}$ cluster, which has an icosahedral structure (C_{5h}). This structure can be considered a core for larger clusters, and then, the number of neon atoms added will gather to build the second solvation layer.

3.2 Relative stabilities

To explore the relative stabilities of the Na^+Ne_n clusters, we have calculated the binding energy per atom E_b , the

second-order difference of energies $\Delta^2 E$ and the fragmentation energies ΔE .

For the pairwise method, the binding energy per atom E_b is calculated by using the following formula:

$$E_b(\text{Na}^+\text{Ne}_n) = -E(\text{Na}^+\text{Ne}_n)/n \quad (4)$$

where $E(\text{Na}^+\text{Ne}_n)$ is the lowest energy corresponding to each cluster.

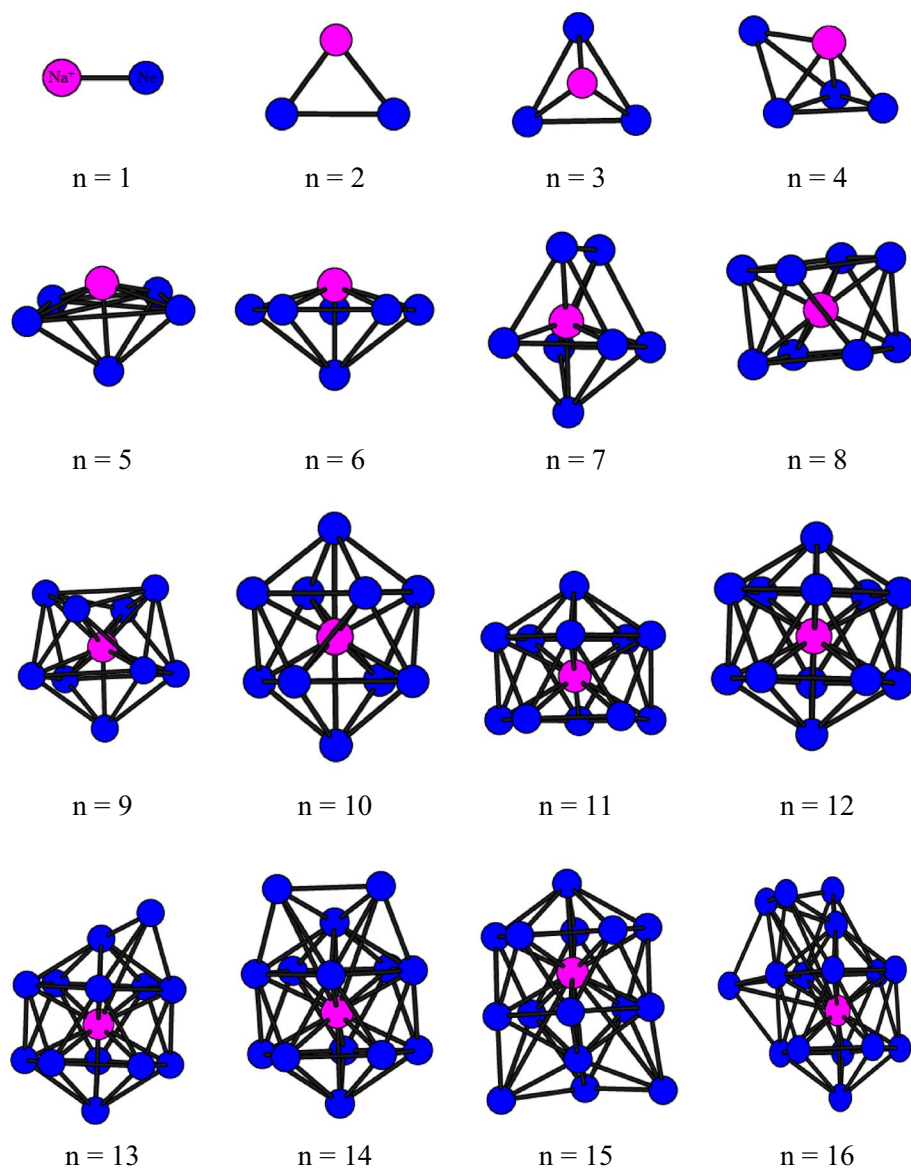
For the DFT calculations, the binding energy per atom E_b of Na^+Ne_n and Ne_n clusters is obtained by using the following formulas:

$$E_b(\text{Na}^+\text{Ne}_n) = [nE(\text{Ne}) + E(\text{Na}^+) - E(\text{Na}^+\text{Ne}_n)]/(n+1) \quad (5)$$

$$E_b(\text{Ne}_n) = [nE(\text{Ne}) - E(\text{Ne}_n)]/n \quad (6)$$

where $E(\text{Na}^+\text{Ne}_n)$, $E(\text{Ne})$ and $E(\text{Na}^+)$ are the lowest energies corresponding to each cluster or atom. The binding energies per atom of Na^+Ne_n and Ne_n are plotted as a function of cluster size as in Fig. 3. For the pairwise method, a pronounced variation is noted for $n = 8$, which expresses the stability of the Na^+Ne_8 cluster. We distinguish an increasing linear behavior up to $n = 8$ which manifests by the domination of

Fig. 2 Lowest energy geometries of Na^+Ne_n clusters calculated with DFT/M06-2X method



$\text{Na}^+\text{--Ne}$ interactions. These clusters continue to gain energy during their growth process. Beyond the first solvation layer, the binding energy per atom decreases progressively with the increase in the cluster size due to the domination of the Ne--Ne interactions. According to the DFT calculations, it can be seen that the binding energy per atom increases with the increase in the cluster size up to $n=9$. The binding energy per atom varies slowly for the clusters with $n=8\text{--}12$, and the curve presents two bumps at $n=9$ and 12, implying that these clusters are more stable than their neighbors.

For pure neon clusters Ne_n , one may observe that their binding energy is lower than that for the mixed Na^+Ne_n clusters. Thus, we can conclude that the doping of the Na^+ cation to the pure Ne_n clusters increases its stability. The second-order difference of energy Δ^2E is a sensitive quantity that reflects the relative stability of clusters, and the results can

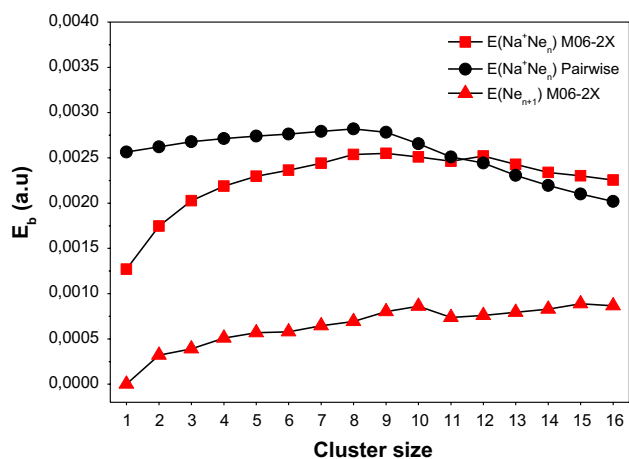
be compared with the relative abundances obtained by using mass spectroscopy analysis. Δ^2E is defined by the following formula:

$$\Delta^2E(\text{Na}^+\text{Ne}_n) = E(\text{Na}^+\text{Ne}_{n+1}) + E(\text{Na}^+\text{Ne}_{n-1}) - 2E(\text{Na}^+\text{Ne}_n) \quad (7)$$

where $E(\text{Na}^+\text{Ne}_{n-1})$, $E(\text{Na}^+\text{Ne}_n)$ and $E(\text{Na}^+\text{Ne}_{n+1})$ represent the total energies of the most stable $\text{Na}^+\text{Ne}_{n+1}$, $\text{Na}^+\text{Ne}_{n-1}$ and Na^+Ne_n clusters. The second-order difference in energies as a function of the cluster size is plotted in Fig. 4. The clusters associated with positive Δ^2E values present a high stability compared to their neighboring clusters. For the DFT method, the most stable clusters are found for $n=5, 8, 9, 10, 12, 13$ and 15. In the case of the pairwise method we note positive peaks for $n=8, 9, 10$ and 12. For both methods, the most pronounced peak of Δ^2E is shown for $\text{Na}^+\text{Ne}_{12}$

Table 2 Structural parameters (in Å) of the Na⁺Ne_n clusters computed with pairwise and DFT methods

Size	Pairwise		DFT	
	Na ⁺ –Ne	Ne–Ne	Na ⁺ –Ne	Ne–Ne
<i>n</i> = 1	2.413	–	2.508	–
<i>n</i> = 2	2.413	3.027	2.529	2.995
<i>n</i> = 3	2.413	3.027	2.514	2.990
<i>n</i> = 4	2.413	3.022	2.535	2.995
<i>n</i> = 5	2.413	3.075	2.535	2.979
		3.000		3.059
		3.964		
<i>n</i> = 6	2.413	3.043	2.556	3.059
		4.080		2.895
<i>n</i> = 7	2.413	3.037	2.529	3.025
		4.075		4.617
<i>n</i> = 8	2.418	2.926	2.519	2.958
		2.974		3.075
<i>n</i> = 9	2.440	2.810	2.519	2.879
		2.905		2.963
<i>n</i> = 10	2.471	2.762	2.836	2.815
	2.524	2.826	2.545	2.974
		3.667		3.239
<i>n</i> = 11	2.477	2.746	2.635	2.794
<i>n</i> = 12	2.588	2.720	2.663	2.799

**Fig. 3** Binding energy per atom of Na⁺Ne_n and Ne_n as a function of the cluster size

cluster implying its high stability, and as a consequence, this cluster is presented at large abundance in mass spectrometry analysis.

Another energetic quantity used to examine the stability of clusters is the fragmentation energy E_f . The fragmentation energy of Na⁺Ne_n and Ne_n clusters is expressed as the following:

$$E_f(\text{Na}^+\text{Ne}_n) = E(\text{Na}^+\text{Ne}_{n-1}) + E(\text{Ne}) - E(\text{Na}^+\text{Ne}_n) \quad (8)$$

The curves are plotted in Fig. 5. As shown in this figure, the most pronounced fragmentation energies are found for Na⁺Ne₈ and Na⁺Ne₁₂. Hence, these clusters are very difficult to be fragmented and they have a lower reactivity with regard to their neighboring clusters which reflect their high stabilities.

The relative stabilities can be discussed by exploring the energy gaps between the highest occupied molecular orbital (HOMO) and lowest unoccupied molecular orbital (LUMO).

$$E_g(\text{Na}^+\text{Ne}_n) = E_{\text{HOMO}}(\text{Na}^+\text{Ne}_n) - E_{\text{LUMO}}(\text{Na}^+\text{Ne}_n) \quad (9)$$

Larger HOMO–LUMO energy gap indicates high chemical stability. Figure 6 displays the energy gap for Na⁺Ne_n clusters as a function of the number of neon atoms.

The energy gap curve of Na⁺Ne_n presents a maximum at *n* = 8 and 12, implying the high stability of these clusters. However, smaller values of HOMO–LUMO gap mean the high chemical reactivity of their corresponding clusters. These facts are similar to those obtained by using binding energy, first-order energy difference, the second-order difference in energy and the fragmentation energy discussed above.

The dipolar properties are of great importance to understand the interatomic interactions and to study electrostatic and optical properties of the clusters. The DFT approach is considered as an interesting method to determine these properties with a good accuracy, contrary to other quantum methods which find many challenges in this determination [58, 59]. The dipole moment as a function of clusters size for the Na⁺Ne_n complexes is computed by DFT method and is depicted in Fig. 7. As clearly seen, all clusters present a polar character except for Na⁺Ne_n (*n* = 8, 9, 10 and 12), which possesses a very weak value of dipole moment, near to zero. The Na⁺Ne₂ cluster presents the highest dipole moment (5.86 D), and then the dipole moment fluctuates as a function of the number of neon atoms and presents an irregular variation. The clusters presenting a large dipole moment have a high charge separation [60]. According to Fig. 7, the Na⁺Ne₈ and Na⁺Ne₁₂ clusters have small values of dipole moment, i.e., a low charge separation due to their high stabilities.

3.3 Topological analysis

The Na–Ne interactions within Na⁺Ne_n clusters are analyzed through a topological atom-in-molecules (AIM) analysis [61]. According to AIM approach, the interaction between two neighboring atoms is characterized by the presence of a bond critical point (BCP). In fact, the presence of the BCP point (3, –1) is indispensable to bind between the two atoms. The topological parameters found at the BCP allow us to conclude about the nature and the strength of such interaction. The electron density

Fig. 4 Variation of second-order energy difference of Na^+Ne_n as a function of cluster size

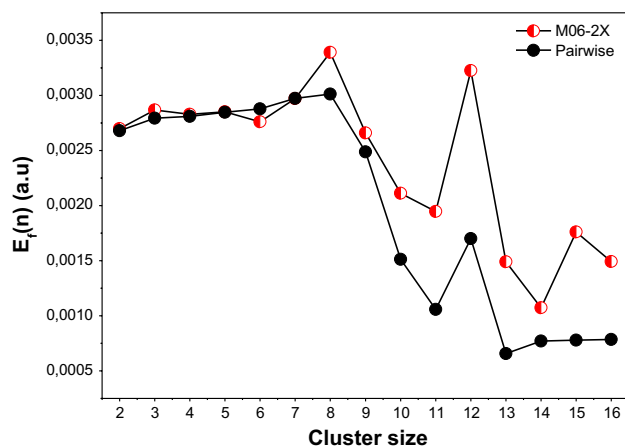
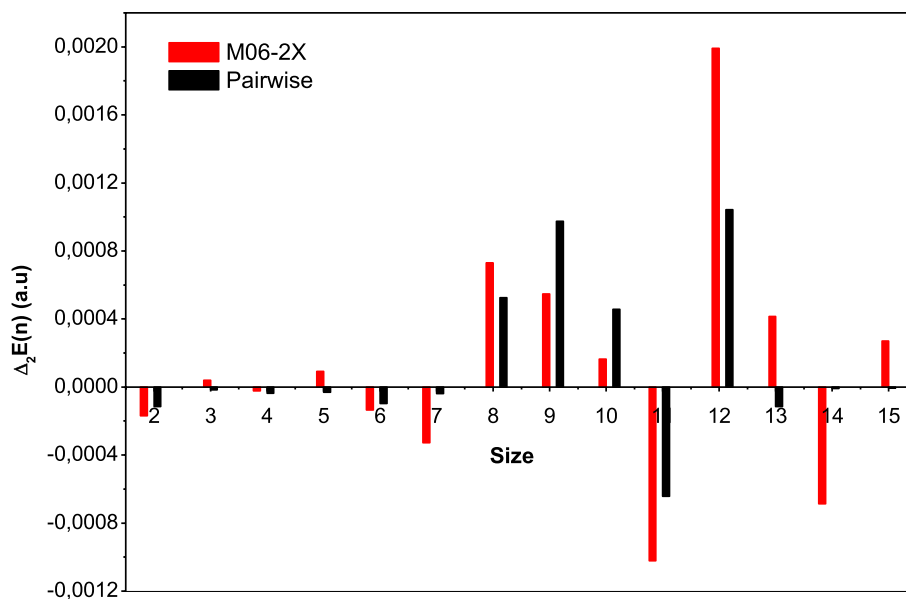


Fig. 5 Variation of fragmentation energy of Na^+Ne_n as a function of cluster size

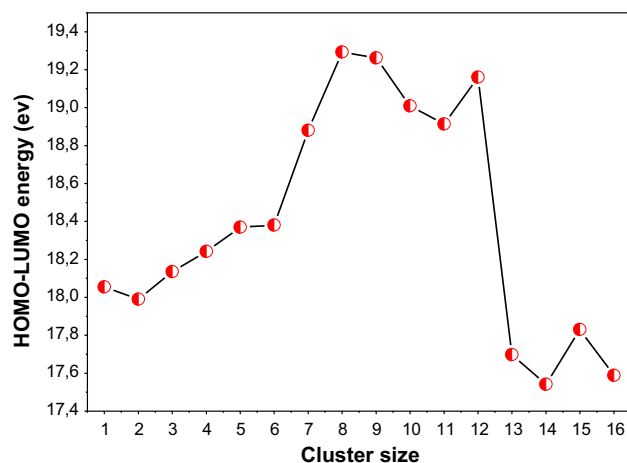


Fig. 6 Variation of HOMO–LUMO energy gap of Na^+Ne_n clusters as a function of the cluster size

ρ_{BCP} and its Laplacian $\nabla^2\rho_{\text{BCP}}$ at a given BCP are the chief parameters. In the AIM approach, the interactions are classified into two types: the closed shell interaction (non-covalent interaction), such as hydrogen bond, ionic and van der Waals interactions, and the shared shell interaction (covalent interaction). The sign of the Laplacian $\nabla^2\rho_{\text{BCP}}$ at the BCP ($3, -1$) is an important indicator which informs about the type of binding. Non-covalent interactions are generally defined by $\rho(r) < 0.1$ a.u. and $\nabla^2\rho(r) > 0$ a.u. [62]. For van der Waals interaction, in requirement to the Pauli exclusion principle the electron density is contracting away from the interatomic surface that allows to low values of electron density of about 10^{-3} a.u. [62]. In Fig. 8, we display the electron density and its Laplacian, respectively, as a function of cluster size. Accordingly,

all electron density values computed at Na–Ne BCPs are smaller, of order of 10^{-3} a.u., and their Laplacian are positive, which confirms the van der Waals interactions within the investigated clusters. The electron density and its Laplacian curves present remarkable peaks for $n = 4$, $n = 8$ and 12. Upper to the last size, these topological parameters appear closely constant. One may conclude that high stabilities of Na^+Ne_8 and $\text{Na}^+\text{Ne}_{12}$ have been proved by the large values of the electron density and its Laplacian compared to their neighboring sizes. The average topological energy $E_{\text{Na-Ne}}$ of the Na–Ne interactions is plotted in Fig. 9. For all studied sizes the values of $E_{\text{Na-Ne}}$ are found in the range of 5 and 10 kJ/mol which confirm the van der Waals interactions between Na and Ne atoms.

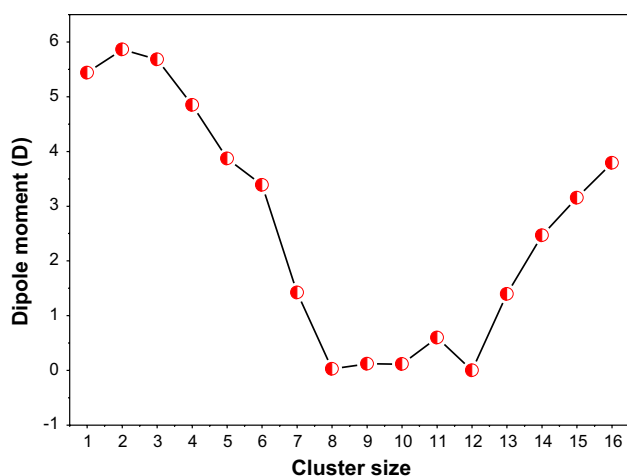
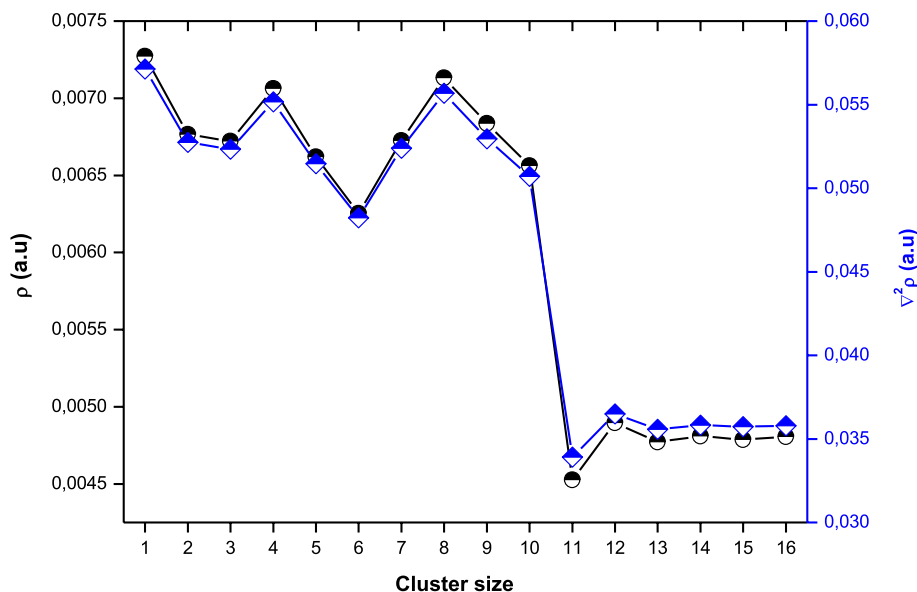


Fig. 7 Dipole moment of Na^+Ne_n as a function of cluster size

The topological energy curve shows pronounced peaks for the sizes $n=4, 8$ and 12 which explain the high stabilities of these clusters. Additionally, the energy density $H(r)$ is a complement indicator to distinguish the type of interactions. The positive values $H(r)$ indicate the non-covalent interactions, and the negative values correspond to covalent interaction. As shown in Fig. 10, our results are typical for non-covalent interactions. It is remarkable that the values of $H(r)$ obtained for Na^+Ne_4 , Na^+Ne_8 and $\text{Na}^+\text{Ne}_{12}$ clusters are greater than those for the neighboring clusters, confirming the previous topological results. Further, another indicator used in this work to confirm the type of interactions is the ratio $G(r)/\rho$ ($G(r)$ is the Lagrangian kinetic energy at the BCP). The values of $\rho(r)$, $G(r)$ and $G(r)/\rho$ are regrouped in Table 3. As reported in this table,

Fig. 8 Size dependence of the electron density and its Laplacian of the Na^+Ne_n clusters



$G(r)/\rho$ values are greater than unity ($G(r)/\rho > 1$) defining the non-covalent binding into the Na^+Ne_n clusters.

3.4 Reduced gradient density

The topological RDG analysis is generally used to identify the nature of intermolecular interactions (such as hydrogen bonding, van der Waals and repulsive steric interactions) [63]. The VMD code provides a visualization of the RDG isosurface in which the type of interactions is determined by color coding: The blue color shows the attractive interactions, the red color is used for the repulsive interactions, and the green color defines the van der Waals interactions. Figure 11 presents the RDG function vs the electron density ρ multiplied by the sign of the second largest value of Hessian matrix of electron density, λ_2 , for the Na^+Ne_n clusters. The position and the width of the observed spikes allow us to conclude about the interatomic interactions within the cluster. Here, the RDG analysis is performed at isosurface equal to 0.5. Obviously, the peaks take place in the range of $[-0.01; 0.005]$ and exhibit well the van der Waals interactions in the Na^+Ne_n clusters. This fact is confirmed by the green color in the RDG isosurface. As seen in Fig. 11, at 0.5 isosurface value, the spikes width varies from one cluster to another. The smaller clusters until $n=12$ possess only one peak localized in the repulsive region ($\lambda_2 > 0$) and two peaks in the attractive region ($\lambda_2 < 0$) closely between -0.002 and -0.01 which are much wider than the repulsive peaks. The attractive effect increases by going to $n=10$ and then decreases for $n=11$. At this size ($n=11$), we remark that the attraction effect is slightly more important than the repulsive one. For $n=12$, equal contributions between attraction and repulsive interactions explain probably the stability of the $\text{Na}^+\text{Ne}_{12}$ cluster. Above this size, the spikes

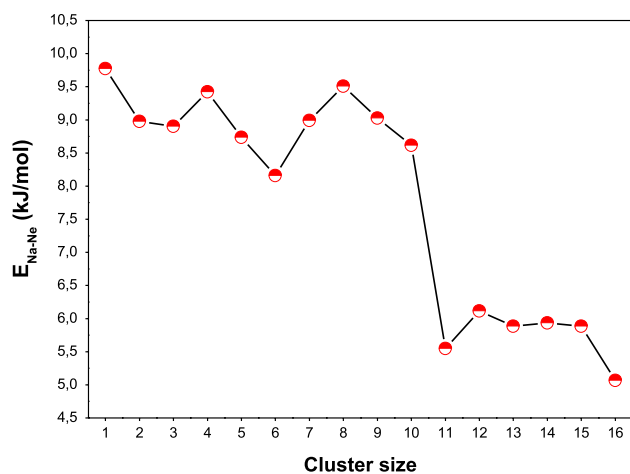


Fig. 9 Variation of the average interaction energy at Na–Ne BCPs as a function of the cluster size

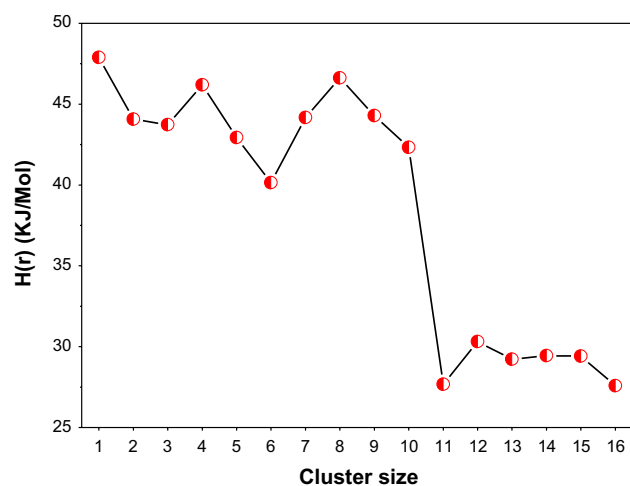


Fig. 10 Variation of the average energy density $H(r)$ as a function of the cluster size

in the attractive region increase again and are larger than the repulsive peaks. These observations are in good agreement with the topological analysis.

4 Conclusions

In this work, we have presented a structural study of the Na^+Ne_n clusters. The geometrical optimization has been carried out by using the pairwise approach and DFT calculation. For the pairwise method, the core–core $\text{Na}^+\text{--Ne}$ potential is fitted by the use of the Tang and Toennies analytical form, and for the Ne–Ne interaction, we used the Lennard-Jones

Table 3 Average values of the electron density $\rho(r)$, the Lagrangian kinetic energy $G(r)$ and the ratio $G(r)/\rho$ at the Na–Ne BCPs of each cluster size

Size n	$\rho(r)$ (a.u.)	$G(r)$ (a.u.)	$G(r)/\rho$ (a.u.)
1	0.0073	0.0109	1.499
2	0.0068	0.0100	1.485
3	0.0067	0.0100	1.483
4	0.0071	0.0105	1.489
5	0.0066	0.0098	1.478
6	0.0062	0.0092	1.466
7	0.0067	0.0099	1.477
8	0.0071	0.0106	1.489
9	0.0068	0.0101	1.475
10	0.0066	0.0096	1.470
11	0.0045	0.0064	1.407
12	0.0048	0.0068	1.416
13	0.0048	0.0067	1.406
14	0.0048	0.0068	1.405
15	0.0048	0.0068	1.418
16	0.0048	0.0067	1.396

potential. The DFT calculation was performed at M06-2X/aug-cc-pVTZ level of theory. For small clusters ($n = 1\text{--}12$), the comparison between the two methods displays systematically the same structures with a small difference in their geometrical parameters except for $n = 6$; the geometry obtained by the DFT is found to be more stable than that in the pairwise method. The first solvation layer is closed at $n = 12$, and it corresponds to the icosahedral structure (C_{5h}). The stability of Na^+Ne_n clusters is discussed in terms of binding energy, first- and second-order derivative energy, fragmentation energy and HOMO–LUMO energy gap. Accordingly, the icosahedral structure $\text{Na}^+\text{Ne}_{12}$ is found to be the most stable cluster. Also, the results show that all Na^+Ne_n clusters present a polar character. The Na^+Ne_8 and of $\text{Na}^+\text{Ne}_{12}$ clusters possess a low value of dipole moment and thus a low charge separation related to the high stability of these clusters. Topological analysis has been performed using the AIM approach, and it gives a positive Laplacian of electron density revealing the van der Waals interaction within the clusters. Reduced density gradient analysis (RDG) was also performed. The RDG plots show the dominance of the attractive effect regarding the repulsive one. Exceptionally for $n = 12$, we note that equal contribution between attractive and repulsive interactions within the $\text{Na}^+\text{Ne}_{12}$ cluster may be responsible to its high stability.

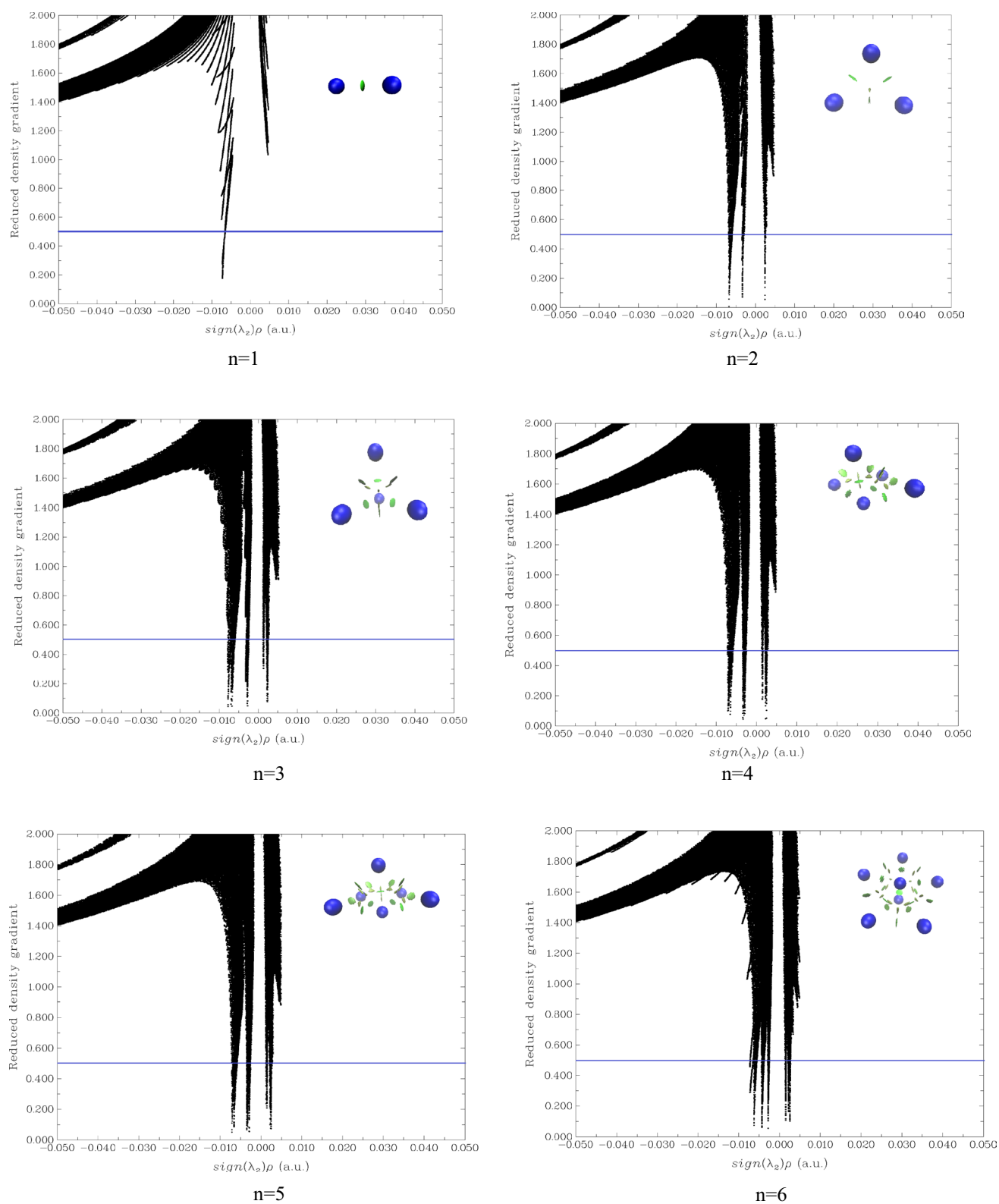


Fig. 11 Reduced density gradient (RDG) function versus the sign of second eigenvalue λ_2 and VMD determination of the RDG isosurfaces (inside plot) for the Na^+Ne_n clusters

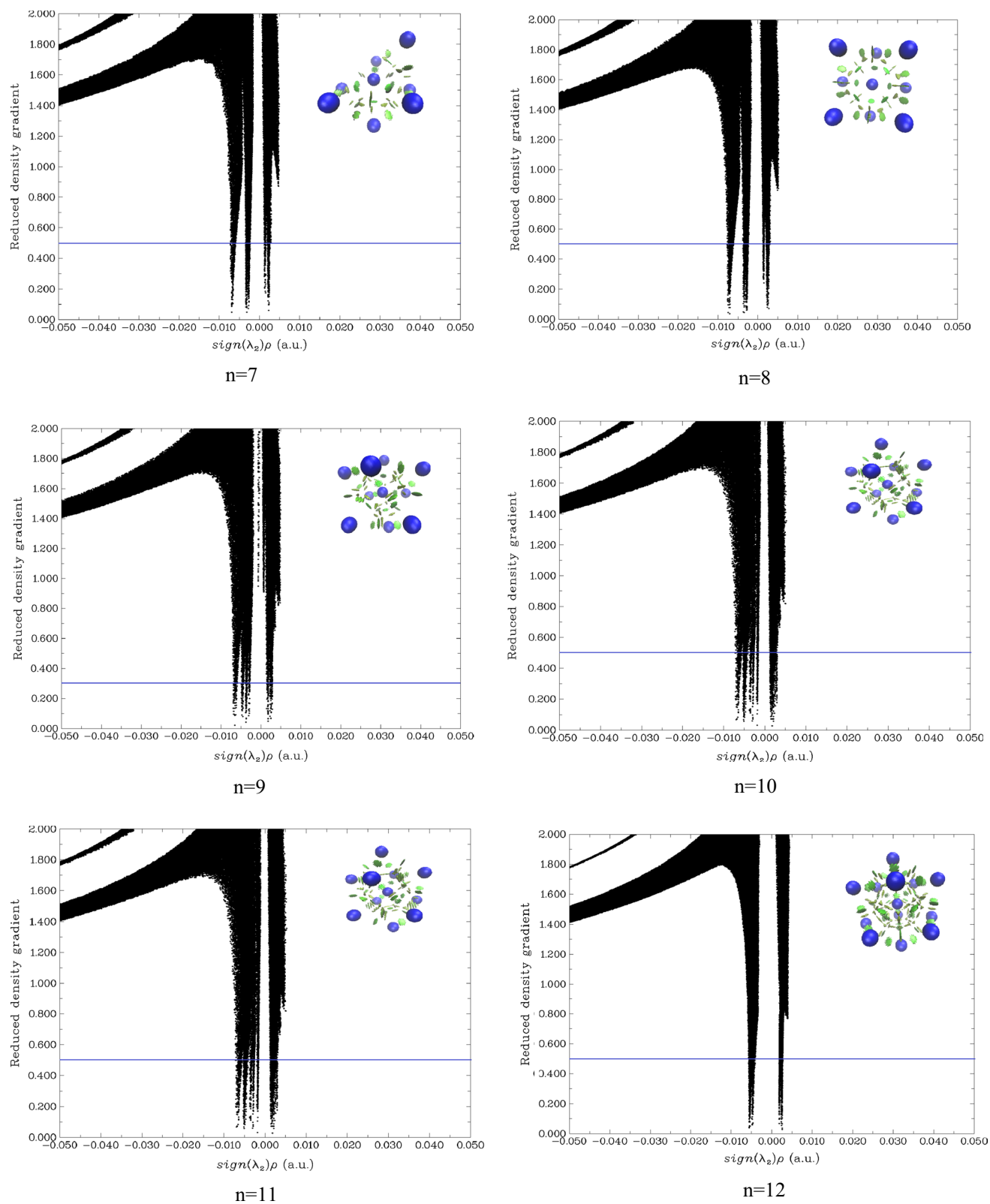


Fig. 11 (continued)

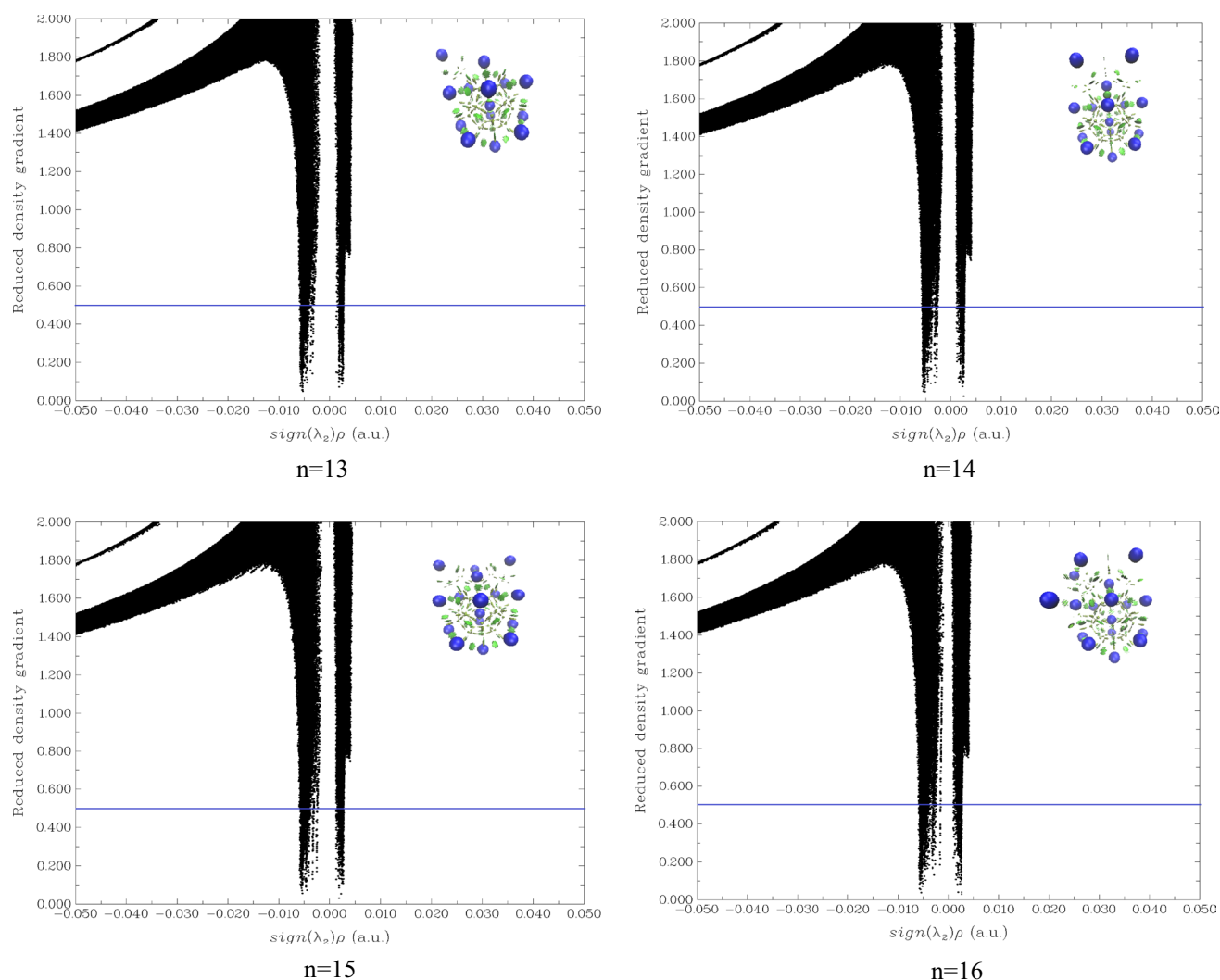


Fig. 11 (continued)

References

- Prekas D, Luder C, Velegarakis M (1997) *J Chem Phys* 108:4450
- Froudakisa GE, Farantos SC, Velegarakis M (2000) *Chem Phys* 258:13
- Ryan M, Collier M, de Pujo P, Crépin C, McCaffrey JG (2010) *J Phys Chem A* 114:3011
- Fanourgakis GS, Farantos SC, Lüder C, Velegarakis M, Xantheas SS (1998) *J Chem Phys* 109:108
- Velegarakis M, Luder C (1994) *Chem Phys Lett* 223:139
- Luder C, Prekas D, Velegarakis M (1997) *Laser Chem* 17:109
- Wright TG, Breckenridge WH (2010) *J Phys Chem A* 114:3182
- Whetten RL, Schriver KE, Persson JL, Hahn MY (1990) *J Chem Soc Faraday Trans* 86:2375
- Farges J, De Feraudy MF, Raoult B, Torchet G (1983) *J Chem Phys* 78:5067
- Farges J, De Feraudy MF, Raoult B, Torchet G (1986) *J Chem Phys* 84:3491
- Gaied W, Ben El Hadj Rhouma M (2011) *Int J Quantum Chem* 111:652
- Issa K, Issaoui N, Ghalla H, Yaghmour SJ, Mahros AM, Oujia B (2016) *J Mol Phys* 114:118
- Bilalbegović G (2003) *Phys Lett A* 308:61
- Di Paola C, Sebastianelli F, Bodo E, Baccarelli I, Gianturco FA (2005) *J Chem Theory Comput* 1:1045
- Sebastianelli F, Bodo E, Baccarelli I, Di Paola C, Gianturco FA, Yurtsever M (2006) *J Comput Mater* 35:261
- Sapse AM, Dumitra A, Jain DCA (2003) *J Clust Sci* 14:21
- Gardner AM, Withers CD, Graneek JB, Wright TG (2010) *J Phys Chem A* 114:7631
- Bu X, Zhong C, Jalbout AF (2004) *Chem Phys Lett* 387:410
- Xinping B, Chongli Z (2004) *Chem Phys Lett* 392:181
- Abdessalem K, Habli H, Ghalla H, Yaghmour SJ, Calvo F, Oujia B (2014) *J Chem Phys* 141:154308
- Hernández-Rojas J, Wales DJ (2003) *J Chem Phys* 119:7800
- Fujisaki A (2002) *J Chem Phys* 117:5271
- Nagata T, Aoyagi M, Lwata S (2004) *J Phys Chem A* 108:683

24. Giju KT, Roszack S, Gora RW, Leszczynski J (2004) *Chem Phys* 391:112
25. Fujisaki A (1995) *J Chem Phys* 102:8485
26. Breckenridge WH, Ayles VL, Wright TG (2007) *Chem Phys* 333:77
27. Lan YZ, Feng YL (2009) *Phys Rev A* 79:033201
28. He J, Wu K, Sa R, Li Q, Wei Y (2010) *Chem Phys Lett* 490:132
29. He J, Wu K, Liu C, Sa R (2009) *Chem Phys Lett* 483:30
30. Issaoui N, Abdessalem K, Ghalla H, Yagmour SJ, Calvo F, Oujia B (2014) *J Chem Phys* 141:174316
31. Gueorguiev GK, Pacheco JM, Stafstrom S, Hultman L (2006) *Thin Solid Films* 515:1192
32. Shi S, Liu Y, Zhang C, Denga B, Jiang GA (2015) *Comput Theor Chem* 1054:8
33. Bhattacharjee D, Mishra BK, Chakrabarty AK, Deka RC (2014) *Comput Theor Chem* 1034:61
34. Liu Y, Tiana Z, Cheng L (2016) *RSC Adv* 6:4705
35. Chuang FC, Hsu CC, Hsieh YY, Albao MA (2010) *Chin J Phys* 48:82
36. Li Z, Zhao Z (2017) *Mater Chem Phys* 187:54
37. Li GL, Ma WL, Gao AM, Chen HY, Finlow D, Li QS (2012) *J Theor Comput Chem* 11:185
38. Maa QM, Xie Z, Wang BR, Liu Y, Li YC (2011) *Solid State Commun* 151:806–810
39. Lin L, Yang J (2015) *J Mol Model* 21:155
40. Wales DJ, Doye JKP (1997) *J Phys Chem A* 101:5111
41. Naumkin FY, Wales DJ (1998) *Chem Phys Lett* 290:164
42. Doye JPK, Wales DJ (1998) *Phys Rev Lett* 80:1357
43. Leary RH, Doye JPK (1999) *Phys Rev E* 60:R6320
44. Naumkin FY, Wales DJ (2000) *Mol Phys* 98:219
45. Wolf MD, Landman U (1998) *J Phys Chem A* 102:6129
46. Xiao Y, Williams DE (1993) *Chem Phys Lett* 215:17
47. Zeiri Y (1995) *Phys Rev E* 51:R2769
48. Deaven DM, Tit N, Morris JR, Ho KM (1996) *Chem Phys Lett* 256:195
49. Ahlrichs R, Böhm HJ, Brode S, Tang KT, Toennies JP (1988) *J Chem Phys* 88:6290
50. Tang KT, Toennies JP (1984) *J Chem Phys* 80:3726
51. Frisch MJ, Trucks GW, Schlegel HB et al (2013) *Gaussian 09, Revision D.01*. Gaussian, Inc., Wallingford, CT
52. Zhang J, Dolg M (2015) ABCluster: the artificial bee colony algorithm for cluster global optimization *Phys. Chem Chem Phys* 17:24173–24181
53. Zhang J, Dolg M (2016) Global optimization of clusters of rigid molecules using the artificial bee colony algorithm. *Phys Chem Chem Phys* 18:3003e10
54. Zhao Y, Truhlar DG (2008) *Theor Chem Acc* 120:215
55. Zhao Y, Truhlar DG (2006) *J Phys Chem A* 110:13126
56. Billings S, Gutowski M, Simons J, Breckenridge WH (1994) *J Chem Phys* 100:8212
57. Aziz RA, Slaman MJ (1989) *Chem Phys* 130:187
58. Reis H, Papadopoulos MG, Boustani I (2000) *Int J Quantum Chem* 78:131
59. Hickey AL, Rowley CN (2014) *J Phys Chem A* 118:3678
60. Dutta A, Mondal P (2017) *Comput Theor Chem* 1115:284
61. Bader RFW (1990) *Atoms in molecules: a quantum theory*. Oxford University Press, Oxford
62. Pakiari AH, Eskandari KJ (2006) *J Mol Struct THEOCHEM* 759:51
63. Johnson ER, Keinan S, Paula MS, Julia CG, Cohen AJ, Yang WT (2010) *J Am Chem Soc* 132:6498

Publisher's Note Springer Nature remains neutral with regard to jurisdictional claims in published maps and institutional affiliations.